# The Effect of Cell Cycle Progression and a Nuclear Localization Signal on CRISPR/Cas9 Gene Correction

**Written by:**
I. Flier
i.flier@students.uu.nl
*Master Student Drug Innovation*

**Daily supervisor:**
D. Wilbie
d.wilbie@uu.nl
*Department of Pharmaceutics, UIPS*

**First examiner:**
Prof. dr. E. Mastrobattista
e.mastrobattista@uu.nl
*Department of Pharmaceutics, UIPS*

**Second Examiner:**
Dr. M. Caiazzo
m.caiazzo@uu.nl
*Department of Pharmaceutics, UIPS*

4th November 2022

Universiteit Utrecht

UIPS Utrecht Institute for Pharmaceutical Sciences

# Abstract

The CRISPR/Cas9 system enables site-specific genome-editing which predominantly occurs via Non-Homologous End Joining (NHEJ), a relatively error-prone pathway. Another pathway is gene correction via Homology Directed Repair (HDR), which can be favoured by presenting an HDR template concomitantly with the Cas9 protein and sgRNA to the cell. Nuclear localization signals (NLSs) can subsequently promote transport of this cargo, encapsulated in lipid nanoparticles (LNPs), into the nucleus. In this work, nuclear localization during different cell cycle stages was determined using a fluorescence-ubiquitin cell cycle indicator (FUCCI) system. Tracking nuclear localization of fluorescently labelled Cas9 over time using confocal microscopy showed that Cas9 enters nuclei predominantly during S/G2/M. Interestingly, the nuclear localization signal did not seem to play a significant role in this process. Even in the presence of ivermectin (0-300µM), a drug inhibiting the process induced by NLS SV40, no significant differences were seen in the occurrence of HDR and NHEJ between samples with and without the NLS. The next goal is to increase the efficiency of nuclear localization of Cas9 through other methods. The human protein phosphatase II (IPP-2) protein for example is primarily taken up during S phase and could thereby stimulate Cas9 uptake during S/G2/M, resulting in an increase in nuclear uptake of Cas9.



**Keywords: CRISPR/Cas9, Homology-Directed Repair, Nuclear Translocation, FUCCI, Lipid Nanoparticles, Nuclear Localization Signal**

# Contents

## Layman's Summary

The CRISPR/Cas9 system works as follows: first, a break is created in one's genetic code. This break can be repaired via different pathways. In the pathway that occurs most often, the two broken pieces are glued together again at random. Since this is a completely random process, it is possible that the genetic code is not restored properly, causing it to dysfunction. To avoid this, one can try to favour another big pathway to repair the break. This pathway uses a piece of genetic code as an example. This piece is replicated and used to fix the break. Since this example is often a replicate of the original piece, the genetic code will be fully restored as it was before the break. It could also be that the example piece is not a replicate of the original piece, but a slightly better version. In this case, the genetic code will end up with this new piece inserted into it, thereby improving it.

A specific protein, Cas9, has to reach the genetic code of a cell for the abovementioned break-and-repair process to start. The genetic code is stored in the nucleus, so the Cas9 has to enter the nucleus. In order to track the protein, it is given a fluorescent label. Next, it is packaged in order to transport it into the nucleus. The transport of the protein into nuclei can be assisted. The protein can be provided with a signal that alerts other elements in the cell that it needs to be transported into the nucleus. This signal is called a 'nuclear localization signal'. However, the performed experiments show that this signal does not help transport of the package as much as expected. Disturbing the signal did not seem to affect the amount of protein that ended up in the nucleus. Also, the presence of this signal did not increase the amount of protein in the nucleus. In order to be able to track the journey of the protein into the cell, the cells are fluorescently labelled as well as the protein, but with a different colour. The cells contain a fluorescent indicator that can tell in which phase of the cell cycle they are. A cell cycle contains four phases, G1, S, G2, and M. If the cells are in G1, they will turn red. When they are in S/G2/M, they will be green.

So, the protein can be tracked and it is possible to visualize during which cell cycle phase the protein enters the nucleus. Results showed that the protein often enters cells when they are green, so when they are in S/G2/M. The next step is to try and improve this, so even more protein enters these cells during this phase. A suggestion for a study like this is to couple this protein to another protein that is mostly taken up during S-phase, so when the cells are green. Hopefully, this will stimulate the protein to enter the green nuclei even more. Another way of increasing protein uptake in the nucleus is by improving the packaging, so less protein is lost and more enters the nucleus where it can exercise its function.

# Abbreviations

| | | |
|---|---|---|
| ApoE | – | Apolipoprotein E |
| Cas9 | – | CRISPR-associated endonuclease 9 |
| CRISPR | – | Clustered Regularly Interspaced Short Palindromic Repeats |
| EMSA | – | Electrophoretic Mobility Shift Assay |
| FUCCI | – | Fluorescence Ubiquitin Cell Cycle Indicator |
| HDR | – | Homology Directed Repair |
| IPP-2 | – | Protein Phosphatase Inhibitor II |
| IVM | – | Ivermectin |
| LNP | – | Lipid Nanoparticle |
| NHEJ | – | Non-Homologous End Joining |
| NLS | – | Nuclear Localization Signal |
| RNP | – | Ribonucleoprotein |
| sgRNA | – | short guide Ribonucleic Acid |

# 1. Introduction

The CRISPR/Cas9 system enables site-specific genome editing. A single guide RNA (sgRNA) guides the CRISPR-associated enzyme Cas9 to a specific site in the genome, where it creates a double-stranded break (DSB) 3 base pairs (bp) upstream of an NGG protospacer adjacent motif (PAM) (1,2). Subsequently, this DSB can be repaired via different pathways, the dominating pathways being Non Homologous End-Joining (NHEJ) and Homology-Directed Repair (HDR) (Figure 1) (3-5). NHEJ mediates direct DSB repair and is able to re-ligate any type of DNA ends, unlike HDR which requires a homologous template to repair the DSB (5,6). As NHEJ does not require a homologous template for the DSB repair, this process can occur throughout the entire cell cycle. This is unlike HDR, which solely occurs during S- and G2-phase when a homologous template of the sister chromatid is available (4,6). As a result of the direct and relatively error-prone re-ligation that occurs during NHEJ, insertions and deletions (indels) might be formed, which can subsequently cause frame-shift mutations and gene knock-out (5,6). Incorrectly repaired DSBs may result in genomic instability and carcinogenesis. Moreover, cells might undergo apoptosis or senescence (6). Under natural circumstances, a sister chromatid is used as homologous template in HDR which ensures correct gene repair, thereby preventing these outcomes (4). Thus, HDR is most often favoured as a repair pathway, even though NHEJ is more prevalent. NHEJ is more prevalent as it occurs throughout the entire cell cycle, it has a dominating nature over HDR, and it is a faster method of gene repair compared to HDR (4).

As mentioned earlier, HDR exclusively occurs during S and G2 phase (6). In 2008, a new method was introduced that enables visualization of cell cycle behaviour of live cells (7,8). Fluorescence Ubiquitin Cell Cycle Indicator (FUCCI) is a technology that acts via two components during cell cycle progression, Cdt1 and Geminin (9). Cdt1 and Geminin are important markers, as their profusion fluctuates during cell cycle progression, in an inverse pattern (Figure 2A). While Cdt1 protein levels peak during G1-phase, right before DNA replication, Geminin levels peak during S-, and G2-phase. Correspondingly, Cdt1 levels decrease abruptly after S-phase initiation, and Geminin levels decrease during late mitosis and G1-phase. The oscillations in expression levels of Cdt1 and Geminin are the result of activation of the E3 ubiquitin ligases APC/CCdh1 and SCFSkp2. The APC/C ubiquitin ligase is active from mid-mitosis throughout G1 and it causes Geminin to degrade. On the contrary,

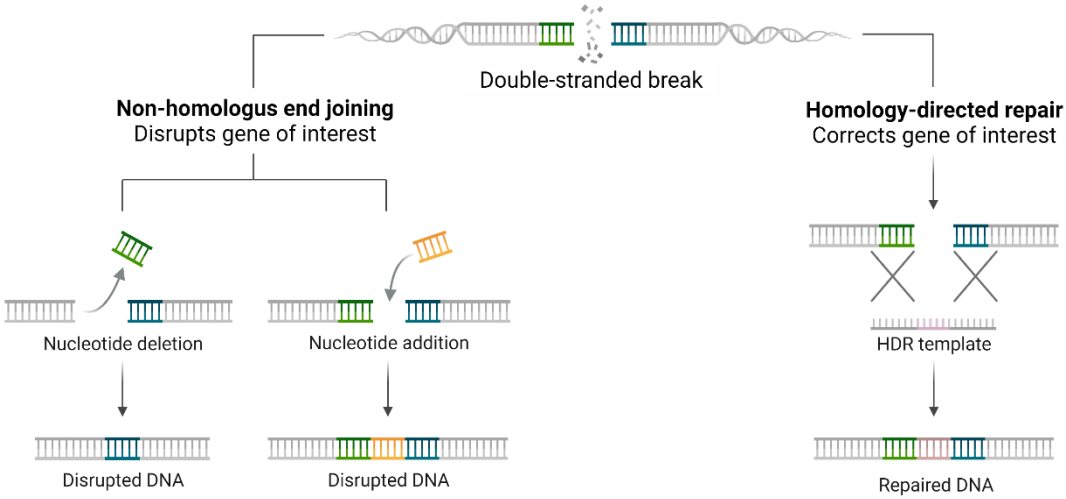


*Figure 1. Schematic overview of the two dominating DSB repair pathways, NHEJ and HDR. NHEJ results in disruption of the gene of interest, while HDR corrects the gene of interest using a homologous template. In this figure, the situation is outlined where a single-stranded HDR template is provided. The figure was adapted from a BioRender template.*

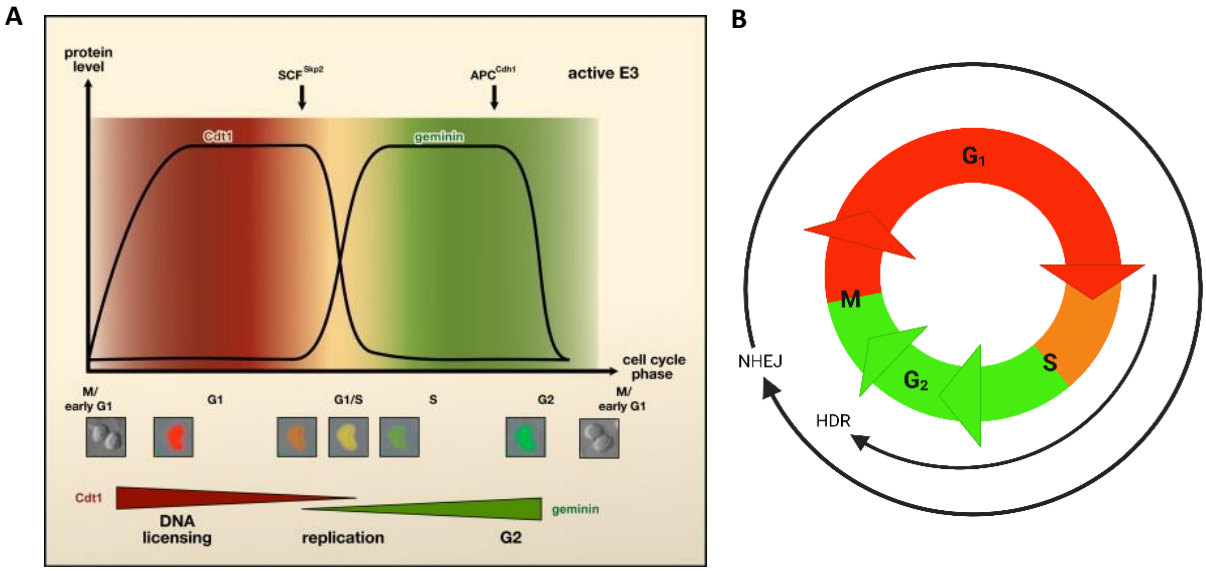


*Figure 2. Figure A shows the inverse pattern in Cdt1 and Geminin profusion, which enables visualization of different cell cycle stages after transduction with the pBOB FastFUCCI plasmid. Figure B represents a schematic overview of cell cycle progression visualized with the FUCCI method. During G1, when Cdt1 levels peak, red fluorescent probes are visualized. During S/G2/M, Geminin peaks and green fluorescent probes are seen. The transition between phases can give an orange signal as both fluorescent probes might be expressed simultaneously by one cell.*

the SCFSkp2 ubiquitin ligase is active during S-, and G2-phase, when it targets the Cdt1 protein for degradation. The reciprocally timed activity of the two ligases can be explained by the fact that SCFSkp2 is a substrate of APC/CCdh1. The FUCCI technique employs pairs of fluorescent proteins fused to degrons derived from Cdt1 and Geminin. During cell cycle progression, these fluorescent proteins are destabilized by APC/C and SCFSkp2 enabling accurate visualization of living cells in either G1 or S/G2/M based on which FUCCI 'probe' is expressed (Figure 2A-B) (8-11).

Introducing an HDR template concomitantly with a ribonucleoprotein complex (RNP) consisting of a Cas9 protein and a single guide RNA (sgRNA) can cause a shift in repair pathway from NHEJ to HDR (4). The HDR template is a specifically designed ssDNA that stimulates HDR of the DSB. The RNP and HDR template can be introduced into a cell by means of a Lipid Nanoparticle (12-15). In order to increase uptake into the nucleus, the Simian Virus (SV)40 Nuclear Localization Signal (NLS) can be incorporated into the Cas9 protein. The SV40 NLS acts as signal fragment to mediate protein transport from the cytoplasm into the nucleus through the nuclear pore complex. This transport is facilitated by members of the importin superfamily (16). In the past decade, scientists have found that Ivermectin (IVM), an anti-parasitic drug that targets the importin superfamily, acts by inhibiting nuclear transport via Imp-α/β1 (17). It works via the same pathway as the SV40 NLS. Hence, theoretically it could block NLS function by inhibiting nuclear transport via Imp-α/β1 (16).

Research has been done to gain controlled nuclear Cas9 delivery. Several methods using protein fusions and small molecule strategies have been experimented with, i.e., Cas9-geminin and nocodazole (18,19). As HDR is predominantly active during S-phase, it could be lucrative to incorporate an S-phase translocating protein into the Cas9 protein. Protein phosphatase inhibitor II (IPP-2) is such an S-phase translocating protein. Thus, a protein fusion of Cas9 and IPP-2 might enhance nuclear translocation of Cas9 during S-phase. It should however be noted that the presence of IPP-2 will cause the cell to prematurely enter mitosis as protein phosphatase I is inhibited by IPP-2 (20-22).

# 2. Materials and Methods

## 2.1 General Reagents

All reagents and chemicals were acquired from Sigma-Aldrich (Zwijndrecht, the Netherlands) unless specified otherwise. sgRNA and (fluorescent) HDR template DNA sequences can be found in Supplementary Table 1. Moreover, 1,1'-((2-(4-(2-((2-(bis(2-hydroxydodecyl)amino)ethyl) (2-hydroxydodecyl)amino)ethyl)piperazin-1-yl)ethyl)azanediyl)bis(dodecan-2-ol) (C12-200) was obtained from CordonPharma (Plankstadt, Germany), 1,2-dioleoyl-sn-glycero-3-phosphoethanolamine (DOPE) was acquired from Lipoid (Steinhausen, Switzerland), Cholesterol and 1,2-dimyristoyl-rac-glycero-3-methoxypolyethylene glycol-2000 (PEG-DMG) from Sigma-Aldrich (Zwijndrecht, The Netherlands), and 1,2-dioleoyl-3-trimethylammonium-propane (DOTAP) from Merck (Darmstadt, Germany). SpCas9 was produced in-house by Danny Wilbie, both with and without an NLS (23).

## 2.2 Lipid Nanoparticle Formulation

The LNPs for HDR-favoured gene correction were formulated by first mixing sgRNA and Cas9 at a 1:1 molar ratio. After 15 minutes of incubation at room temperature, the RNP complex has formed and HDR template (86nt) is added and mixed in a 2:1 molar ratio with the RNP. Concurrently, a lipid mixture was prepared in ethanol (100%). The lipid mixture contains C12-200, DOPE, Cholesterol, PEG-DMG, and DOTAP in a 40:1 (w/w) ratio of lipids to sgRNA (Supplementary Table 2). After complexation of the RNP, the complex is added to the lipid mixture by means of rapid mixture in a 3:1 (v/v) ratio (18 µL RNP + 6 µL lipids). After another 15-minute incubation, the particle has formed with the cargo inside. The final LNPs are diluted four-fold in phosphate buffered saline (PBS). This results in a final RNP molar concentration of 76.9nM in 100µL. A schematic overview of the formulation of these LNPs can be seen in Figure 3.

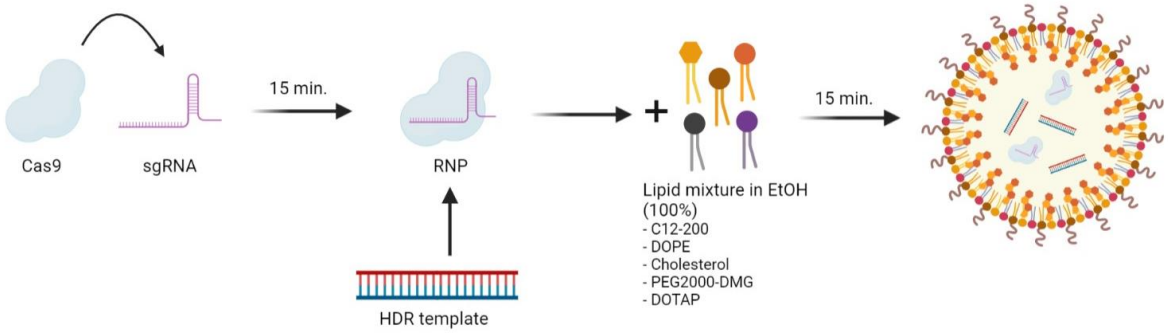


*Figure 3. Schematic overview of the formation of lipid nanoparticles. Cas9 is added to sgRNA and incubated for 15 minutes at room temperature after which HDR template is added. Concurrently, a lipid mixture is prepared. The RNP is added to the lipid mixture by means of rapid mixing and the final LNP is diluted four-fold with phosphate buffered saline. This image was created using BioRender.*

### 2.2.1 Lipid Nanoparticle stability study

To test the stability of the LNPs, the Z-average (d.nm) and polydispersity index (PDI) were measured through dynamic light scattering (DLS) using a Zetasizer Nano S (Malvern ALV CGS-3, Malvern, UK) and Zetasizer Nano Software v3.30. Each sample was measured in triplicate every 24-72 hours. The samples were stored at 4°C in UV-Transparant Disposable Cuvettes (Sarstedt, Etten-Leur, the Netherlands). The cuvettes were closed off using Parafilm (Sigma-Aldrich, Zwijndrecht, the Netherlands).

### 2.2.2. Cargo Encapsulation Efficiency in Lipid Nanoparticles

Encapsulation of the RNP and HDR template in the LNPs was assessed by running an electrophoretic mobility shift assay (EMSA). The rate of complexation of the cargo was determined by loading LNPs onto a Bolt™ 4-12% Bis-Tris Plus gel (1.0 mm x 10 well, Invitrogen, Thermo Fisher Scientific, Carlsbad, USA) and checking whether all separate components (sgRNA, Cas9, and HDR template) remain together or travel different distances. In the case of encapsulation, all cargo components should remain together and not travel far in the gel due to the high molecular weight of the complex. In order to visualize the different components, they were fluorescently labelled. Cas9 was labelled with Cy5-Maleimide (Lumiprobe, Cockeysville, USA), and Atto550-sgRNA and 6FMA-HDR template were used (both were made by Sigma-Aldrich, Zwijndrecht, the Netherlands). The gel was run for 1 hour at 100V using the Bio-Rad PowerPac 300 as energy source.

### 2.2.3. Optimization of the Lipid Nanoparticle Formulation

The composition of the lipid mixture was altered aiming to find the perfect composition (Table 2). Many conditions were prepared, thus each lipid was added at a lower and higher ratio compared to the original formulation (Supplementary Table 2). Finally, the different LNP formulations were prepared and analysed on a Bolt™ 4-12% Bis-Tris Plus gel (1.0 mm x 10 well, Invitrogen, Thermo Fisher Scientific, Carlsbad, USA) in a Bio-Rad mini cell tank using 1X TAE buffer (40mM Tris, 20mM Acetate and 1mM EDTA). Encapsulation was assessed per condition and the best alterations were combined and run again until the best possible ratio of lipids for encapsulation was found. All runs were performed using the Bio-Rad PowerPac 300 at 100V for 1 hour.

Based on the results of this run, that showed that sample 3 achieved higher encapsulation of the cargo compared to the other samples. A new gel layout was prepared (Table 3) where the amount of DOPE and C12-200 was altered, the gel was run similarly to the previous one. Based on the results of this gel, sample 6 was taken for further experiments (Table 3).

A fresh batch of the original formulation and sample 6 were prepared and analysed by performing dialysis overnight in PBS using a Float-A-lyzer G2 device (Amber, 1mL, 12/pkg, Sigma-Aldrich, Zwijndrecht, the Netherlands). Subsequently, fluorescence was measured using the JASCO FP-8300 (Easton, USA) at an excitation wavelength of 493nm and an emission wavelength of 519nm. Fluorescent HDR template was used when preparing the LNPs, so the signal of HDR template could be measured and compared to a similar sample that did not undergo dialysis.

## 2.3. Cell Culture

HEK293T cells and Hepa1-6 cells (both ATCC, Manassas, USA) were cultured in low- and high-glucose DMEM medium (Sigma-Aldrich, Zwijndrecht, the Netherlands) supplemented with 10% foetal bovine serum (FBS), respectively. The cells were cultured at 37°C, 5% $CO_2$. HEK293T-eGFP cells and Hepa1-6-eGFP cells were graciously gifted by Dr. Olivier de Jong and Johanna Walther. The cells were cultured similarly to the WT cells.

Both Hepa1-6 and Hek293T cell lines were transfected with pBOB-EF1-FastFUCCI-Puro plasmid (Addgene #86849). Before transfection and transduction, the plasmid was prepped. It was cultured in LB medium (supplemented with 1% Ampicillin) overnight in a shaking incubator at 37°C, 225 rpm. The next day, this was repeated in greater volumes after which the plasmid was ready for MidiPrep. A MidiPrep was performed using the NucleoBond Xtra Midi EF kit (BIOKÉ, Leiden, the Netherlands). The plasmid was then used for transfection to gain a lentiviral supernatant to be used for transduction. This was done at several lentiviral

supernatant ratios to have at least one properly transduced cell culture. Either 1800µL, 180µL, or 20µL of lentiviral supernatant was pipetted onto 2mL of DMEM medium containing cells at circa 50% confluency in a 6-wells plate. Cells were further cultured and treated with 2µg/mL puromycin (InvivoGen, Toulouse, France) at 37°C, 5% $CO_2$.

Cell culture plastics were acquired from Greiner Bio-One (Alphen aan de Rijn, The Netherlands).

## 2.4. Intracellular Fate of the Lipid Nanoparticle Cargo

To investigate the intracellular fate of the cargo brought into the cells via the LNPs, several studies were performed.

### 2.4.1. Cellular Tracking of Nuclear Uptake

#### *2.4.1.1. BacMam-Nucleus Green Fluorescent Protein as Method For Cellular Imaging*

To visualize nuclei so nuclear uptake of the labelled Cas9 could be visualized, cellular structures of Hepa1-6 cells were imaged using CellLight Reagent Bacmam 2.0 (Thermo Fisher Scientific, Nieuwegein, the Netherlands). On day 0, the cells were seeded at $1.2*10^6$ cells/well in a 48-wells plate using High-Glucose DMEM supplemented with 10% FBS. At day 1, CellLight Reagent Bacmam 2.0 was added at PPC 0, 20, 50, and 100. The expression of the reagent is usually visible from 1 day after addition to the cells onto the $6^{th}$ day after addition. On day 2, the cells were transferred to a 96-wells plate. The cells were counted beforehand using the BioRad TC20 Automated Cell Counter (Hercules, USA) and 20.000 cells/well were transferred to a new well. The cells were incubated overnight (37°C, 5% $CO_2$) and at day 3, the cells were imaged using the Cell Voyager 8000 (Yokogawa, Tokyo, Japan). A control was set-up where the cells were incubated with Hoechst Dye (#33342, 0.2 µg/mL) 15 minutes prior to imaging. Imaging settings can be found in Supplementary Table 3.

#### *2.4.1.2. Identifying Cellular Nuclei and Colocalization using Hoechst Dye*

As the fluorescence of BacMam CellLight reagent only lasts for circa 5 days and it takes 3 days to develop, it could be lucrative to find another method of cellular imaging. As Hoechst dye visualizes DNA, this is an appropriate alternative technique for cell visualization. Cells were incubated with Hoechst dye at room temperature, at least 15 minutes prior to cell imaging in the Cell Voyager 8000. The amount of dye added per well resulted in a final concentration of 0.2 µg/mL.

#### *2.4.1.3. Visualizing Cell Cycle Progression using the FUCCI Technique*

As mentioned before, both Hepa1-6-FUCCI and HEK293T-FUCCI cell lines were constructed using the pBOB-EF1-FastFUCCI-Puro plasmid (Addgene #86849). Using confocal microscopy, the nuclei of these cells could be visualized and nuclear translocation of labelled Cas9 could be tracked per cell cycle stage. Imaging settings can be found in Supplementary Table 3.

### 2.4.2. Fluorescent labelling of Cas9

The intracellular fate of the LNP cargo was tracked by fluorescently labelling the Cas9 protein. 1 mg of Cas9 was labelled with Alexa Fluor 647 C2-maleimide (AF647, Invitrogen, Life Technologies, Eugene, USA) in a 1:20 molar ratio. After overnight incubation at 4°C, the protein was retrieved using a PD-10 column (Sephadex™ G-25 M, Cytiva, Marlborough, USA). The column was rinsed using a four-fold volume excess of Cas9 storage buffer (Supplementary Table 4) prior to adding the sample. The sample was fractionated and the A280 was determined using the NanoDrop One (Thermo Fisher Scientific, Nieuwegein, the Netherlands). Based on these results, the concentration of Cas9 per fraction was calculated and the fractions with the highest concentrations were pooled. Next, 50% glycerol (Sigma-Aldrich, Zwijndrecht, the Netherlands) was added to the sample in a 1:5 (v/v) ratio. The final

concentration was determined using the NanoDrop One and the sample was fractionated into smaller fractions of 50 – 100 µL, depending on concentration. Finally, they were snap-frozen in liquid nitrogen and stored at -80°C.

After labelling, both an activity and purity assay were performed on the newly labelled samples. The activity assay shows Cas9 activity on a piece of linearized DNA (linearized pMJ922, 50 ng/µL) as Cas9 is an enzyme that cuts 1 molecule of DNA per day (single-turnover). Thus, the absolute number of digested DNA molecules in a set time span is an activity measure. Cas9 (1 µM) was mixed with sgRNA (1 µM) in a 1:1 (v/v) ratio and incubated for 10 minutes at room temperature. To this mixture, nuclease activity buffer (NEBuffer 3.1, New England BioLabs, Hitchin, UK), RNAse inhibitor (Thermo Scientific, Vilnius, Lithuania), and nuclease free water were added at a 2:3:1:19 (v/v/v/v) ratio. Finally, 5 µL of pMJ922 plasmid (Addgene #78312) was added and the mixture was incubated for 2 hours at 37°C. After incubation, 1 µL Proteinase K (Thermo Scientific, Vilnius, Lithuania) was added after which the sample was incubated for 1 hour at room temperature. Concomitantly, an 1% agarose gel was prepared, containing Midori Green Advanced DNA Stain (Nippon Genetics, Düren, Germany). Finally, after addition of loading dye (6X orange loading dye, Thermo Scientific, Vilnius, Lithuania), the samples ran for 45 minutes at 100V in 1X TAE buffer (40mM Tris, 20mM Acetate and 1mM EDTA) using the Bio-Rad PowerPac 300. The gel was analysed using the Bio-Rad ChemiDoc Imaging System by imaging Ethidium Bromide for 0.5 seconds.

The purity assay shows whether there are any labelled contaminants present after labelling. 1X Laemlli sample buffer (Bio-Rad, Hercules, USA) was added to the samples and they were incubated for 10 minutes at 70°C. An SDS-PAGE was prepared and ran in 1X Bolt™ buffer (MES SDS Running Buffer, Invitrogen, Thermo Fisher Scientific, Carlsbad, USA) at 100V for 1 hour. The gel was developed using PageBlue Protein Staining Solution (Thermo Fisher Scientific, Carlsbad, USA) and de-stained overnight, after which the results were analysed in the Bio-Rad ChemiDoc Imaging System by imaging Coomassie Blue (automated exposure time).

### 2.4.3. Cellular Uptake of Lipid Nanoparticles in Murine Plasma

Murine Plasma (BL57/6J female mice), graciously gifted by Dr. Marcel Fens, was added to the LNPs to assess the effect of the presence of serum proteins on nuclear translocation of Cas9. The LNPs were incubated for 4 hours with plasma at different ratios serum:LNP (0:1, 1:1, and 4:1). The LNPs incubated with serum were pipetted onto the cells after which they were analysed for 24 hours using the CellVoyager 8000 (Yokogawa, Tokyo, Japan). Data was analysed using Columbus (v2.7.1.). The image analysis settings can be found in Appendix B.

### 2.4.4. Efficacy of the Nuclear Localization Signal in Nuclear Uptake of SpCas9

The in-house produced Cas9 protein contains a SV40 NLS. To assess the effect of this signal on gene correction, ivermectin (IVM) was added in a range of 0 – 300µM. The protocol of this study is schematically explained in Figure 4. Hepa-eGFP cells were seeded (10.000 cells/well) in high-glucose DMEM. After overnight incubation (37°C, 5% $CO_2$), the medium is replaced with similar medium containing IVM (0, 30, or 300 µM). After a one-hour incubation, 20 µL of LNP formulation was added to each well and the cells were incubated for 2 days at 37°C, 5% $CO_2$. Next, the cells were transferred to a 24-wells plate to increase the grow area. After a 5-day incubation, the cells were transferred to a BD Falcon U-bottom 96-well plate (Becton Dickinson, Franklin Lakes, USA) and washed with, consecutively, PBS + 1% BSA, PBS + 1% PFA, and PBS + 1% BSA. Finally, the cell properties were measured using Flow Cytometry (FACSCanto™ II, BD, Franklin Lakes, USA) and analysed using FlowLogic (Inivai Technologies, Mentone, Australia, v7.3.). Cells were first gated in a FSC-A vs. FSC-H plot.

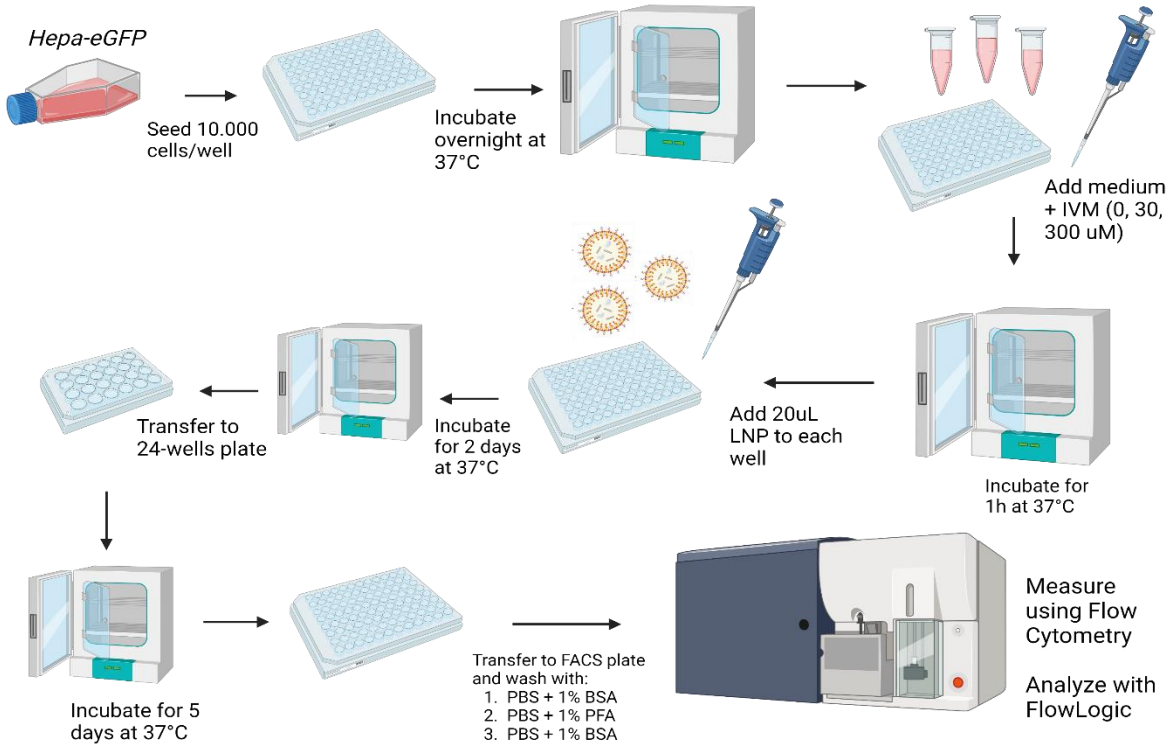


*Figure 4. Schematic Overview of the protocol of the Ivermectin study. DMEM high-glucose medium is replaced with similar medium containing IVM and LNPs are added after a one-hour incubation. Finally, the cell properties were measured using Flow Cytometry.*

Next, single cells were gated in a FSC-A vs. SSC-A plot. Finally, FITC-A signal of the single cells was plotted against Pacific-Blue-A signal (compensation 1% vs. 1%). Cells that underwent NHEJ appeared as double negative in the FITC and Pacific blue channels, while cells that underwent HDR appeared negative for FITC and positive in the Pacific Blue channel (24).

### 2.4.5. The effect of Human Protein Phosphatase Inhibitor 2 on cell cycle progression and nuclear uptake

To study the effect of Human Protein Phosphatase Inhibitor 2 on nuclear translocation in hepatocytes, the protein was labelled with AF647 (1:20 molar ratio), and added to the Hepa-FUCCI cells using Lipofectamine CRISPRMAX Transfection Reagent (Life technologies Corp, Carlsbad, USA). 4 µL of protein solution (100 µg/mL, in PBS) was added to 0.8 µL CRISPRMAX™ Reagent and 20 µL DMEM high-glucose. Nuclear translocation was measured over a period of 72 hours using the CellVoyager 8000 (Yokogawa, Tokyo, Japan) (Supplementary Table 3). Data was analysed in Columbus v2.7.1. (Appendix B)

## 2.5 Statistical Analysis

All statistical analyses were performed in GraphPad Prism v9.4.1. Similarly, all graphs were made using GraphPad Prism v9.4.1. A 2-way ANOVA with multiple comparisons study was performed for the stability assay over time ($\alpha = 0.05$, $^{*}p < 0.05$, $^{**}p < 0.01$, $^{***}p < 0.001$).

# 3. Results

## 3.1 Lipid Nanoparticles

he alterations in the design of the LNPs to improve encapsulation of the cargo showed that an increase in the amount of DOPE (four-fold volume increase) increases encapsulation efficiency of HDR template (Table 2, Figure 5A). In an attempt to increase HDR encapsulation even further, an experiment with varying amounts of DOPE and C12-200 was performed (Table 3, Figure 5B). Based on this study, sample 6 with a C12-200:DOPE ratio of 0.9:1 seemed to result in the highest HDR encapsulation rate. After comparing the encapsulation rate of this sample to the original formulation using dialysis and the JASCO FP-3800 (Table 1), no clear conclusion could be drawn as the original formulation had a higher fluorescent signal after dialysis while sample 6 had a higher fluorescent signal without dialysis. This data is therefore inconclusive. Since altering the lipid composition does not seem to impact HDR encapsulation significantly, it was decided that the original formulation (Supplementary Table 2) would be best for further studies as this formulation had proven its efficacy in past studies (23). Cargo encapsulation in this LNP was tested by adding one fluorescent component out of all three cargo components to the LNP and running these. Results are shown in Figure 5C. It can be seen that not all samples show encapsulation. HDR template and sgRNA seem to bind as they are seen at the same height in the gel. Cas9 however travels further. As Cas9 does not migrate on its own, it does bind to something. Nevertheless, it is unclear what it binds as no other fluorescent signal is seen at the same height as the Cas9. Most likely, the RNP forms and the fluorescence of the sgRNA is obstructed by the Cas9 protein. Since the different fluorescent signals seems to obstruct visualization of each other in the samples, the gel is merely an indication of cargo encapsulation. Lanes 8, 10, and 14 show signs of cargo encapsulation, as cargo is seen at the top of the gel.

*Table 1. Results JASCO measurement of the final samples for LNP optimization (exc./em. 493nm/519nm).*

| Sample | Fluorescence |
|---|---|
| **Dialysis, original formulation** | 7919.2822 |
| **Dialysis, sample 6** | 1188.8088 |
| **No dialysis, original formulation** | 3372.6117 |
| **No dialysis, sample 6** | 6294.1115 |

*Table 2. Overview of different compositions of the LNP for the first gel of the optimization study, see Figure 5A. *0.1% Triton X-100 was added right before adding the LNP to the well **The second original formulation is added for good eyesight comparison with the sample in lane 9, and as validation of the results in lane 1. All volumes are presented in µL.*

| Lane | 1 | 2 | 3 | 4 | 5 | 6 | 7 | 8 | 9 | 10 |
|---|---|---|---|---|---|---|---|---|---|---|
| Name sample | Original formulation (uL) | DOPE low (0.5X) | DOPE high (4X) | Cholesterol low (0.25X) | Cholesterol high (2.5X) | PEG2000-DMG (0.35X) | PEG2000-DMG high (4X) | No LNP | Original formulation + Triton (0.1%)* | Original formulation #2** |
| C12-200 | 0,43 | 0,43 | 0,43 | 0,43 | 0,43 | 0,43 | 0,43 | 0 | 0,43 | 0,43 |
| DOPE | 0,4 | 0,2 | 1,6 | 0,4 | 0,4 | 0,4 | 0,4 | 0 | 0,4 | 0,4 |
| Cholesterol | 1,16 | 1,16 | 1,16 | 0,29 | 2,9 | 1,16 | 1,16 | 0 | 1,16 | 1,16 |
| PEG2000-DMG | 0,62 | 0,62 | 0,62 | 0,62 | 0,62 | 0,22 | 2,48 | 0 | 0,62 | 0,62 |
| DOTAP | 0,44 | 0,44 | 0,44 | 0,44 | 0,44 | 0,44 | 0,44 | 0 | 0,44 | 0,44 |
| EtOH (100%) | 2,95 | 3,15 | 1,75 | 3,82 | 1,21 | 3,35 | 1,09 | 6 | 2,95 | 2,95 |
| Total volume (uL) | 6 | 6 | 6 | 6 | 6 | 6 | 6 | 6 | 6 | 6 |

*Table 3. Lane lay-out of the second gel in the LNP optimization process, see Figure 5B. C12-200 and DOPE volumes are altered.*

| Sample | C12-200 (µL) | DOPE (µL) | EtOH (µL) | Total volume (µL) | C12-200:DOPE (volume ratio) | C12-200 *Compared to original* | DOPE *Compared to original* |
|---|---|---|---|---|---|---|---|
| **1** | 0,43 | 0,4 | 2,96 | 3,79 | 1,08 | 1,0 | 1,0 |
| **2** | 1,99 | 1,8 | 0 | 3,79 | 1,11 | 4,6 | 4,5 |
| **3** | 3 | 0,79 | 0 | 3,79 | 3,80 | 7,0 | 2,0 |
| **4** | 2 | 0,5 | 1,29 | 3,79 | 4,00 | 4,7 | 1,3 |
| **5** | 2,5 | 1 | 0,29 | 3,79 | 2,50 | 5,8 | 2,5 |
| **6** | 1,8 | 1,99 | 0 | 3,79 | 0,90 | 4,2 | 5,0 |
| **7** | 0,79 | 3 | 0 | 3,79 | 0,26 | 1,8 | 7,5 |
| **8** | 0,5 | 2 | 1,29 | 3,79 | 0,25 | 1,2 | 5,0 |
| **9** | 1 | 2,5 | 0,29 | 3,79 | 0,40 | 2,3 | 6,3 |
| **10** | 0,43 | 0,4 | 2,96 | 3,79 | 1,08 | 1,0 | 1,0 |

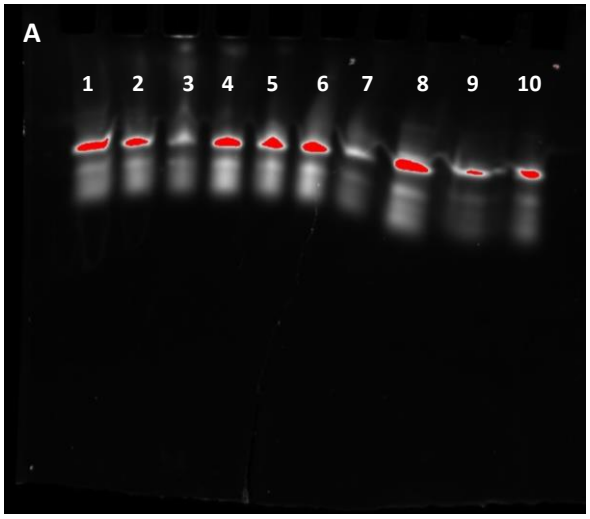


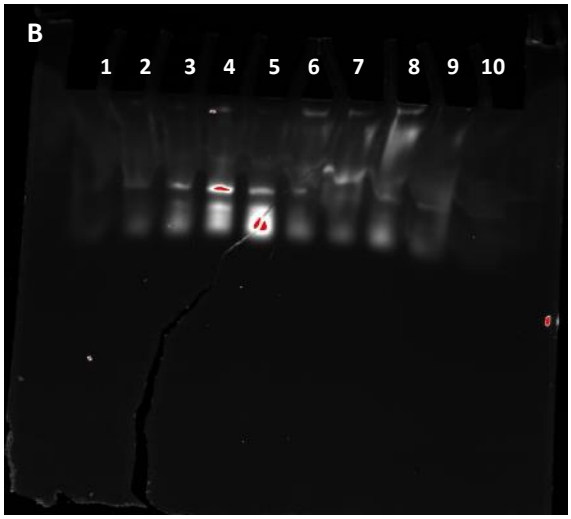


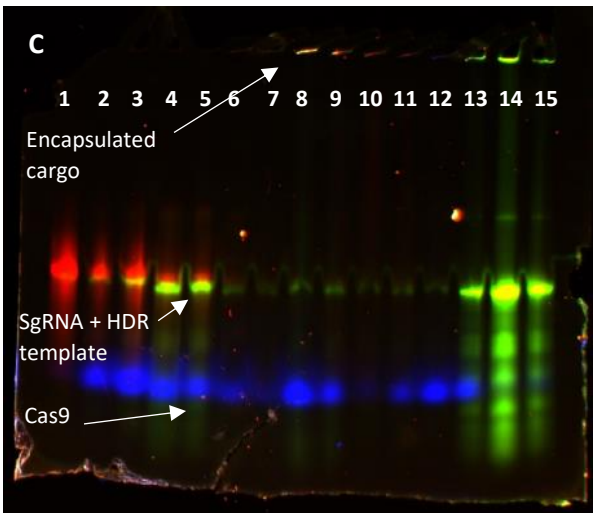


| Lane | sgRNA | Cas9 | HDR | Lipid mixture |
|---|---|---|---|---|
| **1** | Fluo | - | - | - |
| **2** | - | Fluo | - | - |
| **3** | Fluo | Fluo | - | - |
| **4** | Fluo | Fluo | Fluo | - |
| **5** | - | - | - | - |
| **6** | Fluo | Fluo | Fluo | Yes |
| **7** | - | - | - | - |
| **8** | Fluo | Fluo | Fluo | Yes + EtOH (100%) |
| **9** | - | - | - | - |
| **10** | Fluo | Regular | Regular | Yes |
| **11** | - | - | - | - |
| **12** | Regular | Fluo | Regular | Yes |
| **13** | - | - | - | - |
| **14** | Regular | Regular | Fluo | Yes |
| **15** | - | - | - | - |

*Figure 5. Gel A shows the results of the first step in the LNP optimization process. Gel B shows the second step, with only C12-200 and DOPE volumes altered. Gel C shows the results of the encapsulation assay of the final LNP formulation and its cargo. Red signal represents ATTOsgRNA, blue represents fluorescent Cas9 and green the fluorescent HDR. Lane outlines of gel A-C can be found in Table 1, 2, and 4, respectively. The table shows the gel lay-out of gel C.*

### 3.1.1. Lipid Nanoparticles remained stable over a period of fourteen days

To test whether the prepared LNP formulations could be stored for several days, a stability study was performed in which the PdI and Z-average (d.nm) of two batches of LNP formulations were monitored over time, while stored at 4°C. During this study, the LNP formulations were stored in a fridge at 4°C. The PdI of both LNPs did not show a significant change throughout the measuring period (Figure 6A). However, as shown in Figure 6B, the Z-average did significantly increase since day 0, in both samples. Nevertheless, as the values remained in the range that was deemed appropriate for the LNP, it was decided the LNPs could be kept throughout the week, so for a 5-day period. This period was used as a maximum storage period for all following studies.

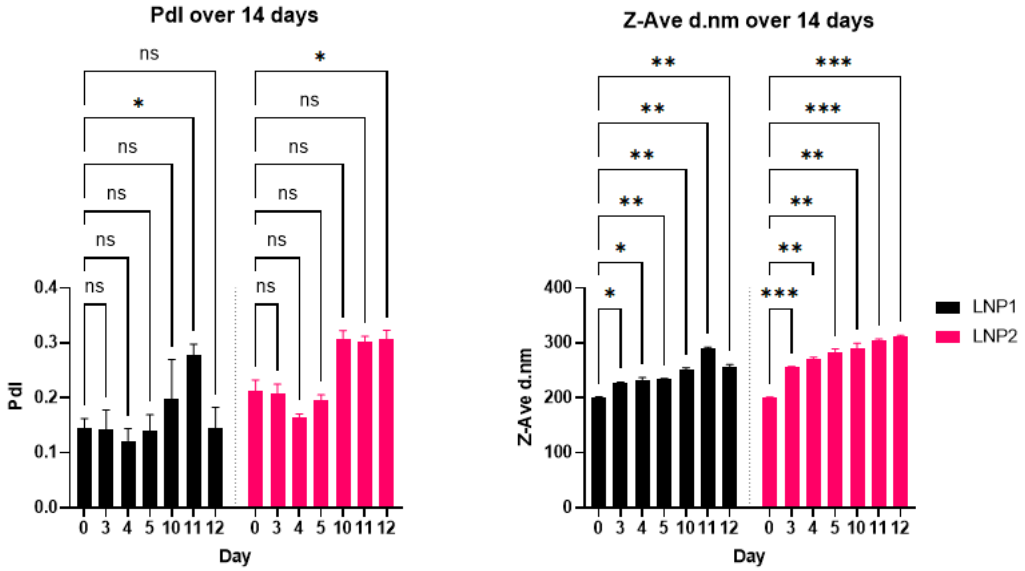


*Figure 6. Stability study of the Lipid Nanoparticles. Figure 6A shows the Polydispersity Index (PdI) over time, 6B shows the size of the LNPs in A-average (d.nm) over time. N = 3. α = 0.05, *p < 0.05, **p < 0.01, ***p < 0.001.*

## 3.2. Intracellular Fate of the Lipid Nanoparticle Cargo

### 3.2.1. Labelled Cas9 showed no contaminant labelled proteins, nor any activity

As shown in Figure 7A, Cas9 loses its activity after labelling to AF647. However, as can be seen in unlabelled Cas9 sample with NLS, its baseline activity was low. In the indicated box, a light second band can be seen which indicates protein activity. As this is a very light band, thereby showing low baseline activity, it could be that the assay was not too good since the protein did show activity in other experiments.

Figure 7B shows there are no contaminant labelled proteins after labelling. The protein can thus be used to study the nuclear translocation as it can be visualized properly.

### 3.2.2. Cellular Imaging techniques

Visualization using BacMam Nucleus CellLight Reagent was not suitable for our experiments. Only a small fraction of the cells was fluorescently labelled and thus visible. Moreover, the signal disappeared within 5 days, which means the cells had to be labelled on a weekly basis, a process that takes up to 3 days. Hence, it would be more lucrative to find a more efficient or long-lasting technique to visualize the cells.

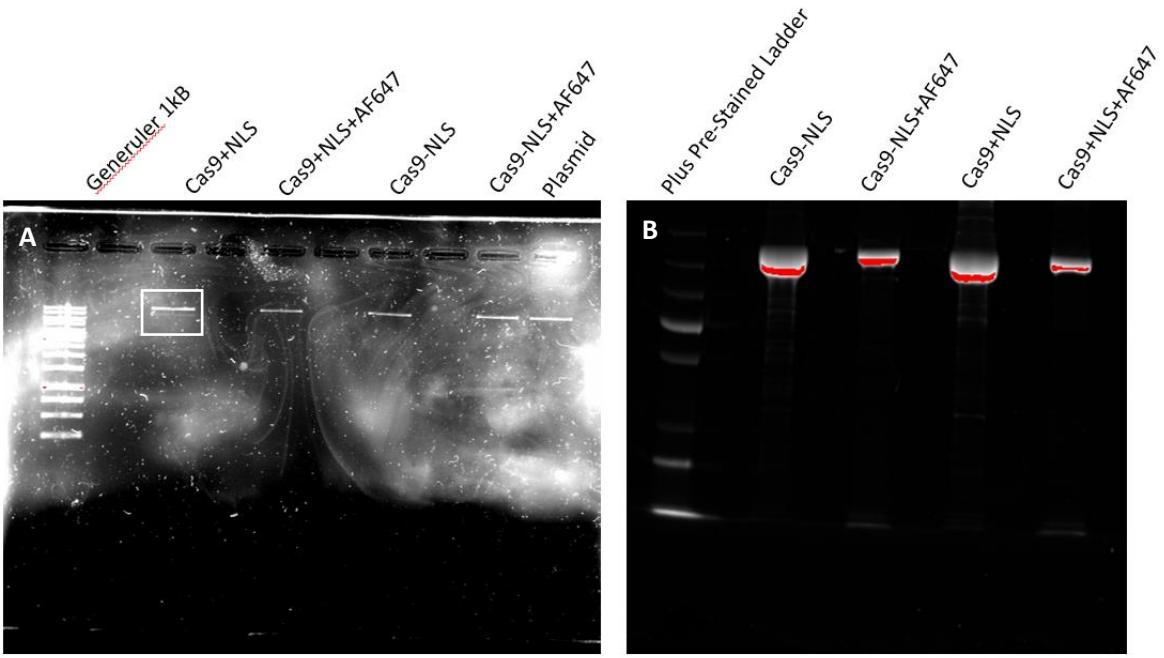


*Figure 7. An activity assay (gel A) of the labelled Cas9 with and without NLS shows that Cas9 is inactive after labelling. It shows the same results as the plasmid, the negative control. The purity assay (gel B) ensures that there are no contaminations in the protein after labelling. For neither the Cas9+NLS, nor Cas9-NLS.*

Hoechst dye did seem to efficiently visualize nuclei. However, during the longer uptake studies, the cells went into apoptosis. As this was not seen in the Brightfield images of the negative control, this is most likely a negative effect of the Hoechst dye. Moreover, Hoechst dye interfered with the fluorescent signal of the ATTOsgRNA. Therefore, nuclear translocation could not properly be assessed.

### 3.2.3. Murine Serum Negatively Affects the Cas9 Uptake into the Cells

As the therapy will be administered intravenously, the effect of serum proteins on the LNP formulation was assessed. Incubation of the LNPs with serum at different ratios shows that the visualization of fluorescent Cas9 is more difficult after incubation with serum. Whether this happens due to a quenching effect or a possible effect the serum proteins might have on the LNPs is unclear. However, as shown in Figure, to properly assess nuclear translocation of Cas9, it is better not to incubate the LNPs with serum.

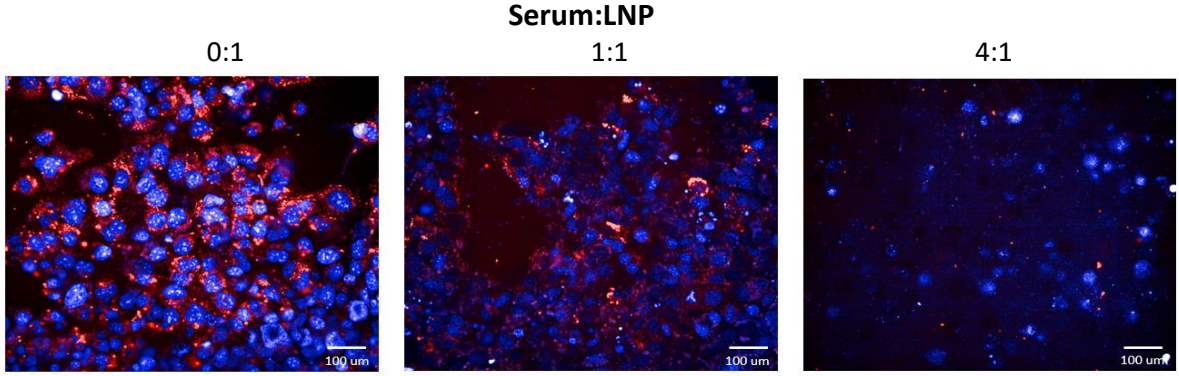


*Figure 8. The effect of adding murine plasma on Cas9 uptake in hepatocytes. The nuclei are visualized with Hoechst (blue) and Cas9 is labelled with Cy5-Maleimide (red). N = 240 – 1101 nuclei per well. The scale bar indicates a distance of 100µm.*

### 3.2.4. pBOB FastFucci Plasmid Visualizes Cell Cycle Progression

After transfection of Hepa1-6 cells with the pBOB FastFUCCI plasmid, the nuclei express either green or red fluorescence, based on cell cycle progression (Figure 9A-D). The red nuclei represent cells that are in phase G1 of the cell cycle , while the green nuclei represent cells in S/G2/M.

### 3.2.5. Nuclear Translocation of Cas9

As shown in Figure 9A-C, Cas9 (yellow signal) migrates into the nuclei of cells. Figure 9FigureD shows that after 56 hours, hardly any cells are visible anymore. This could be an indication of cytotoxicity of the LNPs or simply apoptosis after almost three days of incubation in the same medium. Graph 9E shows that nuclear uptake of Cas9 achieves maximum nuclear uptake during S/G2/M circa 48 hours after addition of the LNPs to the cells. The signal in cells in G1 peaked circa half a day later regarding nuclear Cas9 uptake. This could be explained by the fact that the cells that were in S/G2/M have moved into G1 phase by now, or the earlier peak during S/G2/M could be a result of the absence of a nuclear barrier during S/G2. The uptake may be simple diffusion into the nucleus instead of NLS-mediated. Both aforementioned explanations could justify the trend we see in nuclear translocation per cell cycle phase. Finally, Graph 9F shows nuclear translocation of Cas9 over time. It can be seen that nuclear translocation occurs earlier in cells in S/G2/M and peaks around the same time as nuclear uptake. Cells in G1 however show a higher and quicker nuclear translocation rate.

#### *3.2.5.1. Nuclear Localization Signal SV40*

Figure 10 shows nuclear uptake and translocation of Cas9, with and without a NLS, per cell cycle phase. As shown in Figure 10A, nuclear uptake of Cas9 occurs first during S/G2/M, regardless of the presence of a NLS. Circa 1 day later, nuclear uptake peaks in cells in G1, also regardless of NLS presence. Nuclear translocation was calculated by taking the ratio between nuclear and cytosolic Cas9 uptake. At a nuclear translocation rate of y = 1, a similar

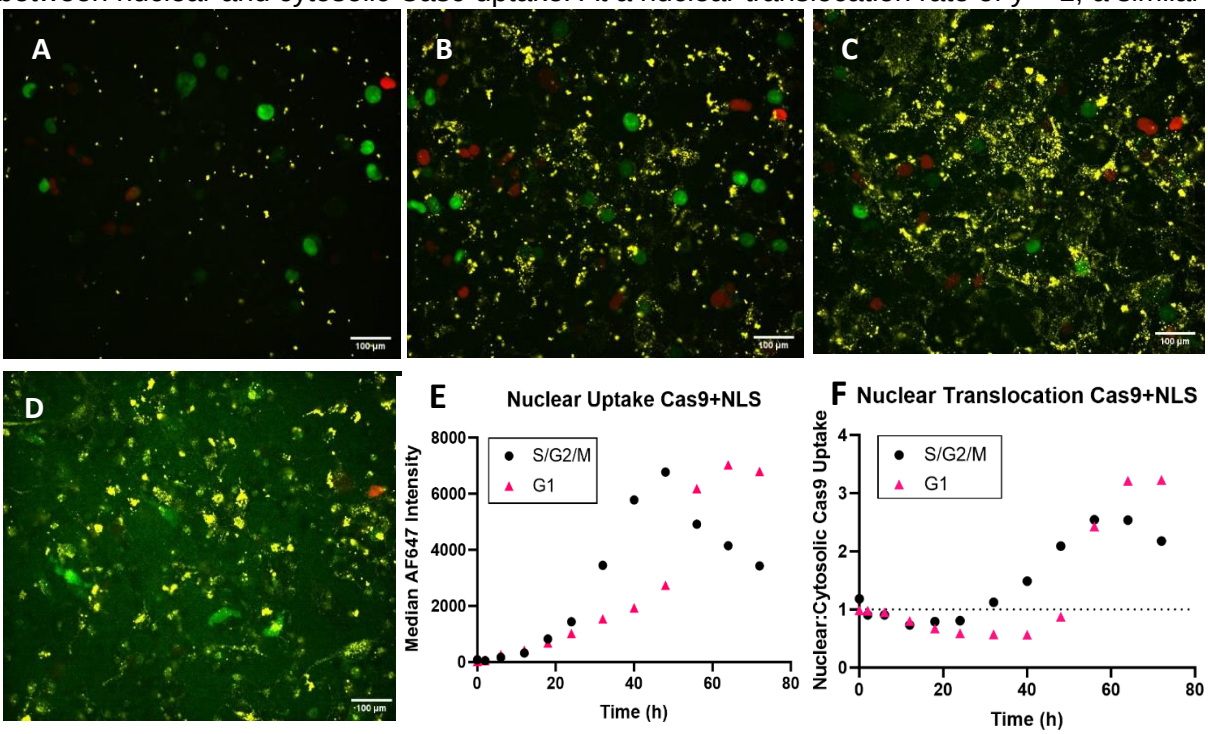


*Figure 9. Nuclear translocation visualized in Hepa1-6 FUCCI cells over time. (A) t = 0h, (B) t = 18h, (C) t = 40h, (D) t = 56h. Red nuclei indicate cells in G1, and green nuclei indicate cells in S/G2/M. Cas9 is labelled with AF647, which can be seen in yellow in figures A-D. Graph E shows the Nuclear Uptake of Cas9 per cell cycle phase. Graph F shows the Nuclear Translocation, this was calculated by dividing the nuclear uptake of Cas9 by the cytosolic uptake. At y = 1, the nuclear and cytosolic uptake are equal. If y > 1, Cas9 is migrating into the nucleus. N = 866 – 3277 nuclei per well. The scale bar indicates a distance of 100µm.*

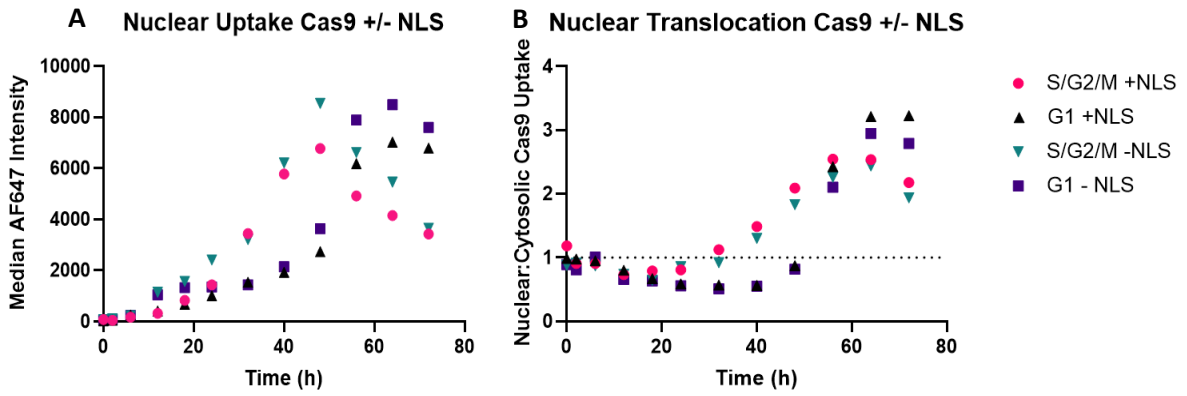


*Figure 10. Nuclear uptake and translocation in hepa1-6 FUCCI cells of Cas9 with and without a Nuclear Localization Signal. Graph A shows the nuclear uptake of Cas9 +/- NLS per cell cycle phase, graph B shows nuclear translocation of the Cas9 +/- NLS per cell cycle phase, this was calculated by dividing the nuclear uptake of Cas9 by the cytosolic uptake. At y = 1, the nuclear and cytosolic uptake are equal. If y > 1, Cas9 is migrating into the nucleus. N = 866 – 3277 nuclei per well.*

amount of Cas9 is present in the nucleus as in the cytosol. If y > 1, Cas9 is travelling into the nucleus. Figure 10B shows that after about 1.5 days, Cas9 starts entering the nuclei of cells in S/G2/M. This process starts slightly later for cells in G1, as they reach y > 1 after circa 2 days, when cells in S/G2/M are at the peak of nuclear translocation.

### *3.2.5.2. Ivermectin as Nuclear Localization Signal Pathway Inhibitor*

Figure 11 shows that increasing the concentration of IVM does not correlate with the amount of HDR editing, no clear trend is found. The relative amount of HDR editing between samples with and without NLS seems to differ less at 300 µM compared to 30 µM. Nevertheless, this difference is very small. The relative amount of HDR editing within the corrected values of this experiment does give the impression that an increase in IVM concentration weakens the effect

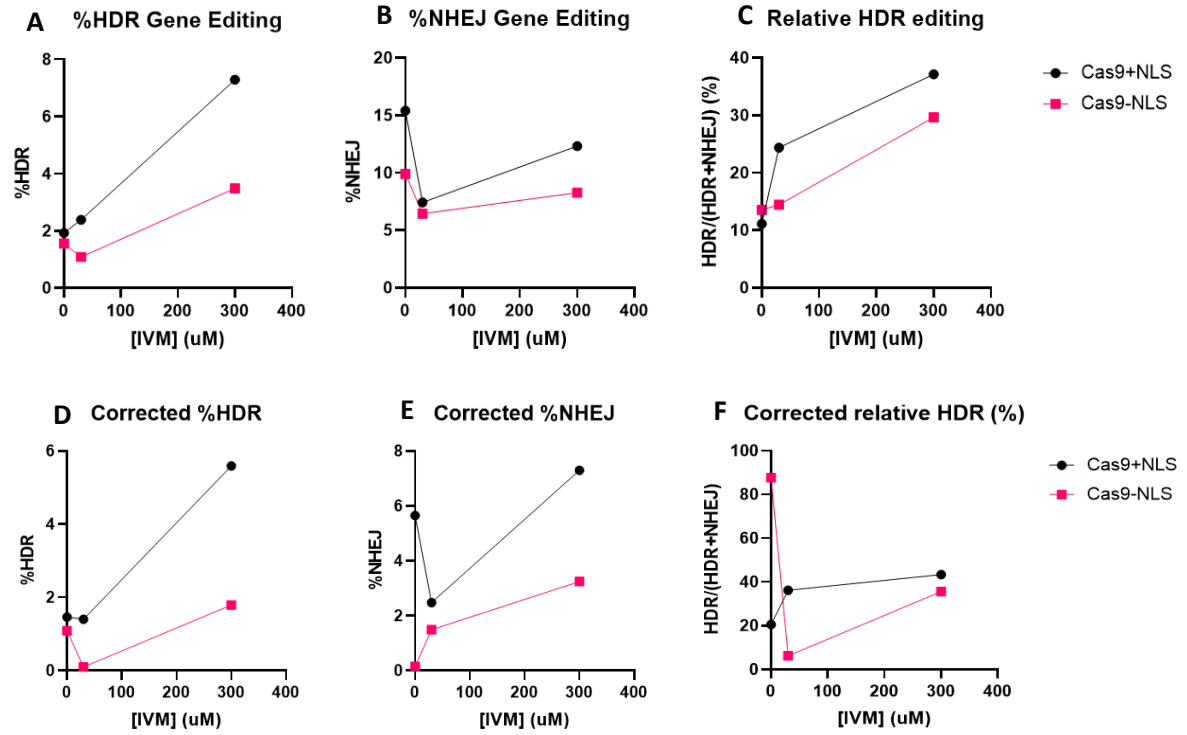


*Figure 11. The effect of an increasing dose of Ivermectin on NHEJ and HDR gene-editing. Graphs D-F were corrected with PBS samples. N = 5885 – 9990 events per condition; 1-2 wells per condition.*

of the NLS. However, no clear trend can be seen here either. The graphs do not show any linear or dose-responsive correlation between the amount of HDR editing and the concentration of IVM.

### 3.2.6. Human Protein Phosphatase Inhibitor 2

As can be seen in 12A, both nuclear and cytosolic uptake of IPP-2, a potential S-phase translocation marker, increase at circa 40h after addition of the protein to the cells. The steepest increase can be seen in cells that are in S/G2/M phase. However, at t = 10h, we see a spike in IPP-2 intensity in cells in G1, concerning both nuclear and cytosolic IPP-2 uptake. Figure 12B shows nuclear translocation of the protein over time. The results indicate a small advantage for nuclear translocation during S/G2/M over time.

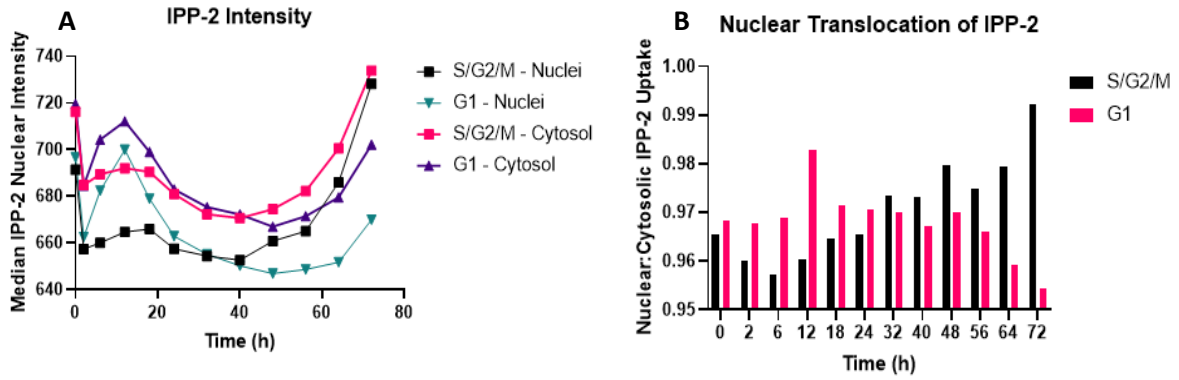


*Figure 12. Expression of IPP-2 after addition to Hepa1-6 Fucci cells using a Lipofectamine Kit. Graph A shows nuclear and cytosolic uptake of the protein, which was labelled with AF647. Graph B shows nuclear translocation of IPP-2, this was calculated by dividing the nuclear uptake of Cas9 by the cytosolic uptake. N = 886 – 3750 nuclei per well.*

# Discussion

After experimenting with the composition of the LNPs, it was found that the original formulation was the best formulation to continue with. Even though it seemed that increasing the relative amount of DOPE resulted in increased HDR encapsulation, later studies showed this was not necessarily the case. Thus, it was decided to carry on with the lower DOPE concentration. However, when running a gel with fluorescent cargo components, it was seen that there were still cargo components not encapsulated. Thus, there is room for improvement. Moreover, visualization of the HDR template seemed to be an issue so other methods should be looked into for quantification of HDR encapsulation in the LNP. After this, HDR encapsulation can be improved further if deemed necessary. Higher encapsulation rates will save materials as a bigger portion of cargo reaches its destination. However, an LNP formulation was necessary to continue with experiments which is why further optimization was put on hold. More studies into possibly altering the LNP composition and accurate quantification of HDR encapsulation should be carried out, since no reliable quantification could be performed based on the gel. This could be explained by a possible quenching effect of the signal caused by the ethanol present in the sample.

As one of the interests of this research regards nuclear uptake of the cargo, the Cas9 protein was fluorescently labelled. After labelling of Cas9 with AF647-maleimide, a purity study showed no labelled contaminants in the samples. However, the activity assay indicated low to none Cas9 activity. Especially peculiar was the fact that the protein showed very low baseline activity, even though it was active in other experiments. This could indicate an issue in the activity assay and it should therefore be repeated with a positive control. To study nuclear translocation, the activity did not matter as much. Experiments measuring relative HDR and NHEJ gene engineering however could be affected by this matter. Thus, these experiments may need to be repeated if it appears that the activity assay did show accurate results and the Cas9 activity is very low.

Before using cells that express the FUCCI plasmid, different techniques were tried out to image the nuclei of the cells in order to track nuclear translocation of Cas9. The first effort was made with BacMam Nuclear CellLight Reagent. However, this ended quickly due to several reasons. The main reason being that nuclei of cells treated with this reagent were only visible for a few days and that this technique requires quite some work for a visualization of merely a few days. However, this meant a new imaging technique had to be thought of and applied. One of the standard ways of visualizing nuclei is by using Hoechst dye. This is a dye that binds DNA and shows blue fluorescence. This was our next step, but as we continued our experiments, we saw that over time, the dye seemed to negatively affect our LNPs and cells, thereby our results were invalid. This was particularly clear during uptake studies over time, where Hoechst dye seemed quite toxic to the cells after a while. This was a big disadvantage and a solid reason to search for a new method. It was decided to incorporate the pBOB FastFUCCI plasmid in the genome of the cells. After transduction of the cells with this plasmid, cells started expressing green and red fluorescent signals based on cell cycle stage. Thus, it could be concluded that incorporation of this plasmid into the cell genome was a success.

The effect of serum proteins on LNPs was assessed as LNPs are opsonized in serum and coated with apolipoprotein E (ApoE) following intravenous administration (25,26). However, during the serum incubation study, results indicated that incubating the LNPs with serum prior to addition to the cells caused diminished view of Cas9 translocation as the Cy5 signal (fluorescent label of the Cas9 protein) got weaker as the ratio serum:LNP increased. Furthermore, less nuclei were visible and the background signal of the Hoechst dye seems greater when the ratio serum:LNP is higher. Regardless of the bad visualization of Cas9, which

disturbs the results, this also indicates possible cytotoxicity. An explanation for this may be that in the bloodstream, there is continuous movement. In the well plate however, this is not the case. The LNPs that were incubated with serum were added to the cells after which no more movement occurs. Nevertheless, it should not be forgotten that Hoechst dye was shown to have a negative effect on the cells over time during the nuclear translocation studies over time. This should be remembered while drawing any conclusions regarding the effect of the serum. So, studies were also performed where serum was added to Hepa-FUCCI cells as no Hoechst dye was necessary here. However, no clear conclusions could be drawn from this study as the serum still affected fluorescence of the labelled Cas9.

Nuclear uptake of Cas9 in the Hepa-Fucci cell line peaked at circa 48 hours after addition of the LNPs to the cells. At this moment, nuclear translocation in cells in S/G2/M was also at its highest. About 12 hours later, cells in G1 reached their nuclear translocation peak. As hepatocytes divide once per 24 hours, this 12-hour delay of nuclear translocation peak in G1 cells can be explained by progression of mitosis. The cells that peaked at t = 48h are then moving into G1, at which time the apparent nuclear translocation in G1 phase increases. The nuclei already contain Cas9, causing the nuclear over cytosolic uptake rate to increase. This pattern of synchronization can be read out of the graphs. However, as mentioned before, the trend we see in the graphs could also be caused by diffusion of Cas9 into the cells during S/G2, as the nuclear membrane is disrupted during these stages of the cell cycle. Also, since nuclear uptake peaks after 48 hours, experiments that were recorded over a period of 24 hours should be repeated and performed for a longer period of time, i.e. 60 hours, in order to be sure to record maximal nuclear translocation of Cas9 and the effect hereof.

A remarkable finding is that the trend in both nuclear uptake and nuclear translocation do not seem to differ much, regardless of the presence of an NLS. The question that comes to mind is whether this NLS actually contributes to nuclear translocation. Thus, another experiment was designed to test this.

As mentioned, ivermectin is a drug that destabilizes the cargo-importin α complex that is formed in reaction to the presence of an NLS. As opposed to the natural process, where importin β1 subsequently binds to the complex after which it travels into the nucleus through the nuclear pore complex, the cargo-importin α complex is destabilized, thereby no complex with importin β1 is formed which is expected to result in less to no transport into the nucleus via the nuclear pore complex. In other words, one would expect that an increasing dose of ivermectin would continue to decrease the function of the NLS, thereby decreasing nuclear Cas9 uptake overall, except when the nuclear membrane is disrupted during the G2/M phase and passive diffusion becomes possible. Accordingly, this was tested in a study with increasing doses of ivermectin. Total HDR and NHEJ were measured and analysed. As the NLS should lose its function as ivermectin concentration increases, one would expect the differences in relative HDR gene correction between the sample with and without an NLS to get smaller. In spite of these expectations, no clear trend was to be seen in the results. This could be explained by a series of reasons. First of all, during this experiment many different steps need to be performed by hand. There could be some human error in this. Furthermore, the *n* of this pilot study was low (*n* = 1-2), the experiment should be repeated in triplo at least. Additionally, no activity assay was performed on the Cas9 used for this study beforehand, thus it is not sure how high the activity of the used protein is. As the performed activity assay of Cas9 showed lower activity than expected, it should be taken into account that the Cas9 might not function as well as expected. However, as mentioned before, this could also be an issue in the activity assay. Finally, the results were based on a study were 40 µL of LNPs was added to each well. In all previous experiments, this was merely 20 µL and these studies gave even

more inconclusive results. Hence, moving forward more studies should be executed using at least 40 µL LNPs. An LNP titration could also be performed to find the optimal dosing.

Finally, a pilot study was performed using protein phosphate inhibitor II. It was expected that this protein would be taken up during S phase, thus nuclear uptake should peak in S/G2/M. The results do indicate slightly more nuclear translocation in S/G2/M cells over time, but this difference is too small to draw any conclusions at this stage. A peak is also seen in both nuclear and cytosolic uptake in G1 cells quite soon after adding the protein to the cells, it takes longer before the protein is taken up in S/G2/M cells, even though both nuclear and cytosolic uptake are higher in S/G2/M than G1 in the end. This experiment still has a lot of options for optimization. Different strategies than using the lipofectamine CRISPRMax kit could be examined. ProDeliverIN CRISPR might be a good alternative. Moreover, a titration should be performed to find the appropriate volume of IPP-2 to add. Also, this experiment has only been performed once, it should be repeated for validity. After optimizing the delivery strategy, the next step is to perform a protein fusion. As IPP-2 is expected to principally enter nuclei during S-phase, a protein fusion resulting in Cas9-IPP-2 may result in increased nuclear translocation of Cas9 as nuclear uptake during S/G2 will increase due to the presence of IPP-2.

In conclusion, nuclear translocation of Cas9 predominantly occurs during S/G2/M-phase of the cell cycle. Addition of an NLS to the Cas9 protein does not seem to significantly increase this rate. Remarkably, the presence of an NLS shows no apparent effect on nuclear Cas9 uptake in different cell cycle stages. It could be hypothesized that the use of an NLS is obsolete in this case. Nevertheless, the aforementioned suggested studies should be performed and the performed studies should be repeated before any final conclusions on exclusion of the use of NLSs in nuclear translocation can be drawn. As discussed before, there are several other ways to improve nuclear translocation. Unfortunately, our pilot study did not show significant nuclear translocation of IPP-2 on itself. However, changing the method of protein addition to the cells could change this. Instead of using the Lipofectamine kit, ProDeliverIN CRISPR may be a good alternative. Moreover, gene fusion resulting in Cas9-IPP-2 should be performed to assess a possible increase in nuclear translocation of Cas9 during S/G2.

# References

(1) Wilbie D, Walther J, Mastrobattista E. Delivery Aspects of CRISPR/Cas for in Vivo Genome Editing. Accounts of chemical research 2019 Jun 18,;52(6):1555-1564.

(2) Liu M, Zhang W, Xin C, Yin J, Shang Y, Ai C, et al. Global detection of DNA repair outcomes induced by CRISPR–Cas9. Nucleic acids research 2021 Sep 7,;49(15):8732-8742.

(3) Wright WD, Shah SS, Heyer W. Homologous recombination and the repair of DNA double-strand breaks. The Journal of biological chemistry 2018 Jul 6,;293(27):10524-10535.

(4) Yang H, Ren S, Yu S, Pan H, Li T, Ge S, et al. Methods Favoring Homology-Directed Repair Choice in Response to CRISPR/Cas9 Induced-Double Strand Breaks. International journal of molecular sciences 2020 Sep 4,;21(18):6461.

(5) Mao Z, Bozzella M, Seluanov A, Gorbunova V. Comparison of nonhomologous end joining and homologous recombination in human cells. DNA repair 2008;7(10):1765-1771.

(6) Davis AJ, Chen DJ. DNA double strand break repair via non-homologous end-joining. Translational cancer research 2013 Jun;2(3):130-143.

(7) Sakaue-Sawano A, Kurokawa H, Morimura T, Hanyu A, Hama H, Osawa H, et al. Visualizing Spatiotemporal Dynamics of Multicellular Cell-Cycle Progression. Cell 2008;132(3):487-498.

(8) Zielke N, Edgar BA. FUCCI sensors: powerful new tools for analysis of cell proliferation. Wiley interdisciplinary reviews. Developmental biology 2015 Sep;4(5):469-487.

(9) Méchali M, Lutzmann M. The Cell Cycle: Now Live and in Color. Cell 2008;132(3):341-343.

(10) Sakaue-Sawano A, Kurokawa H, Morimura T, Hanyu A, Hama H, Osawa H, et al. Visualizing Spatiotemporal Dynamics of Multicellular Cell-Cycle Progression. Cell 2008;132(3):487-498.

(11) Koh S, Mascalchi P, Rodriguez E, Lin Y, Jodrell DI, Richards FM, et al. A quantitative FastFUCCI assay defines cell cycle dynamics at a single-cell level. Journal of cell science 2017 Jan 15,;130(2):512-520.

(12) Juliano RL, Ming X, Carver K, Laing B. Cellular Uptake and Intracellular Trafficking of Oligonucleotides: Implications for Oligonucleotide Pharmacology. Nucleic acid therapeutics 2014 Apr 1,;24(2):11-113.

(13) Suzuki Y, Onuma H, Sato R, Sato Y, Hashiba A, Maeki M, et al. Lipid nanoparticles loaded with ribonucleoprotein–oligonucleotide complexes synthesized using a microfluidic device exhibit robust genome editing and hepatitis B virus inhibition. Journal of controlled release 2021 Feb 10,;330:61-71.

(14) Dinah W. Y. Sah, Ka Ning Yip, Alexander Klibanov, Liu Liang Qin, Antonin de Fougerolles, William Cantley, et al. Lipid-Like Materials for Low-Dose, in vivo Gene Silencing. Proceedings of the National Academy of Sciences - PNAS 2010 Feb 1,;107(5):1864-1869.

(15) Wei T, Cheng Q, Min Y, Olson EN, Siegwart DJ. Systemic nanoparticle delivery of CRISPR-Cas9 ribonucleoproteins for effective tissue specific genome editing. Nature communications 2020 Jun 26,;11(1):3232.

(16) Lu J, Wu T, Zhang B, Liu S, Song W, Qiao J, et al. Types of nuclear localization signals and mechanisms of protein import into the nucleus. Cell communication and signaling 2021 May 22,;19(1):60.

(17) King CR, Tessier TM, Dodge MJ, Weinberg JB, Mymryk JS. Inhibition of Human Adenovirus Replication by the Importin α/β1 Nuclear Import Inhibitor Ivermectin. Journal of virology 2020 Aug 31,;94(18).

(18) Lin S, Staahl BT, Alla RK, Doudna JA. Enhanced homology-directed human genome engineering by controlled timing of CRISPR/Cas9 delivery. eLife 2014 Dec 15,;3:e04766.

(19) Matsumoto D, Tamamura H, Nomura W. A cell cycle-dependent CRISPR-Cas9 activation system based on an anti-CRISPR protein shows improved genome editing accuracy. Communications biology 2020 Oct 23,;3(1):601.

(20) BRAUTIGAN DL, SUNWOO J, LABBE J-, FERNANDEZ A, LAMB NJC. Cell cycle oscillation of phosphatase inhibitor-2 in rat fibroblasts coincident with p34cdc2 restriction. Nature (London) 1990;344(6261):74-78.

(21) Wang W, Stukenberg PT, Brautigan DL. Phosphatase Inhibitor-2 Balances Protein Phosphatase 1 and Aurora B Kinase for Chromosome Segregation and Cytokinesis in Human Retinal Epithelial Cells. Molecular Biology of the Cell 2008 Nov 1,;19(11):4852-4862.

(22) Kakinoki Y, Somers J, Brautigan DL. Multisite Phosphorylation and the Nuclear Localization of Phosphatase Inhibitor 2-Green Fluorescent Protein Fusion Protein during S Phase of the Cell Growth Cycle. The Journal of biological chemistry 1997 Dec 19,;272(51):32308-32314.

(23) Walther J, Wilbie D, Tissingh VSJ, Öktem M, van der Veen H, Lou B, et al. Impact of Formulation Conditions on Lipid Nanoparticle Characteristics and Functional Delivery of CRISPR RNP for Gene Knock-Out and Correction. Pharmaceutics 2022 Jan 17,;14(1):213.

(24) Glaser A, McColl B, Vadolas J. GFP to BFP Conversion: A Versatile Assay for the Quantification of CRISPR/Cas9-mediated Genome Editing. Molecular therapy. Nucleic acids 2016;5(7):e334.

(25) Akinc A, Maier MA, Manoharan M, Fitzgerald K, Jayaraman M, Baros S, et al. The Onpattro story and the clinical translation of nanomedicines containing nucleic acid-based drugs. Nature nanotechnology 2019 Dec 4,;14(12):1084-1087.

(26) Akinc A, Querbes W, De S, Qin J, Frank-Kamenetsky M, Jayaprakash KN, et al. Targeted Delivery of RNAi Therapeutics With Endogenous and Exogenous Ligand-Based Mechanisms. Molecular Therapy 2010 Jul;18(7):1357-1364.

# Supplementary Materials

## Appendix A: Supplementary Data

*Supplementary Table 1. DNA sequences of used materials*

| ***Sample*** | ***Sequence*** |
|---|---|
| ***Fluorescent HDR template*** | *[6FAM]C*AAGCTGCCCGTGCCCTGGCCCACCCTCGTGACCACCCTGAGCCACG GCGTGCAGTGCTTCAGCCGCTACCCCGACCACATGAAGC |
| ***sgRNA*** | GCUGAAGCACUGCACGCCGU |
| ***HDR template*** | CAAGCTGCCCGTGCCCTGGCCCACCCTCGTGACCACCCTGAGCCACGGCGT GCAGTGCTTCAGCCGCTACCCCGACCACATGAAGC |

*Supplementary Table 2. Lipid Nanoparticle Formulation.*

| **Lipid** | **Mw (g/mol)** | **Molarity needed (mM)** | **Volume (uL)** |
|---|---|---|---|
| **C12-200** | 1136.96 | 1.45 | 0.43 |
| **DOPE** | 744.03 | 0.66 | 0.40 |
| **Cholesterol** | 386.65 | 1.93 | 1.16 |
| **PEG2000-DMG** | 2000 | 0.10 | 0.62 |
| **DOTAP (diluted 50x)** | 663.1 | 0.01 | 0.44 |
| **Total volume lipids** | 746.77305 | 4.14 | 3.04 |
| **EtOH (100%)** | | | 2.96 |
| **Total volume lipid mixture** | | | 6.00 |

*Supplementary Table 3. CellVoyager 8000 imaging settings per target*

| **Target** | **Method** | **Fluorophores** | **Objective** | **Light source** | **Acquisition** | **Exposure time (ms)** | **Binning** |
|---|---|---|---|---|---|---|---|
| **Bright Field** | Brightfield (confocal path) | NA | 40x | Lamp | BP525/50 | 200 | 4x4 |
| **Hoechst** | Confocal Fluorescence 405/488/561/640 nm | Not specified | 40x | 405 nm | BP445/45 | 1000 | 4x4 |
| **Red Signal (FUCCI)** | Confocal Fluorescence 405/488/561/640 nm | Not specified | 40x | 561 nm | BP600/37 | 1000 | 4x4 |
| **Green Signal (Bacmam eGFP/FUCCI)** | Confocal Fluorescence 405/488/561/640 nm | Not specified | 40x | 488 nm | BP525/50 | 250 | 4x4 |
| **Cy5** | Confocal Fluorescence 405/488/561/640 nm | Not specified | 40x | 640 nm | BP676/29 | 2500 | 4x4 |
| **AF647** | Confocal Fluorescence 405/488/561/640 nm | Not specified | 40x | 640 nm | BP676/29 | 750 | 4x4 |

*Supplementary Table 4. Recipe Cas9 Storage Buffer (6X)*

| Cas9 storage buffer (6X) | Component | Calculation amounts needed |
|---|---|---|
| | **60 mM Tris** | Cas-nr: 77-86-1 (Trizma base)<br>MW Tris: 121,14 g/mol<br>7,27 gram |
| | **1800 mM NaCL** | MW NaCl: 58,44 g/mol<br>105,19 gram |
| | **0.6 mM EDTA** | Cas-nr: 6381-92-6<br>Mw: 372,24 g/mol<br>223 mg |

## Appendix B: Image Analysis Columbus v2.7.1.

### Analysis Sequence "220912 IF Hepa Fucci 72h uptake"

| | | | |
|---|---|---|---|
| **Input Image** | **Stack Processing :** Individual Planes<br>**Flatfield Correction :** None | | |
| **Find Image Region** | **Channel :** BP525/50 (1)<br>**ROI :** None | **Method :** Whole Image Region | Output Population : Whole Image<br>Output Region : Whole Image Region |
| **Find Cells** | **Channel :** BP525/50 (3)<br>**ROI :** Whole Image<br>**ROI Region :** Whole Image Region | **Method :** B<br>Common Threshold : 0.1<br>Area : > 80 µm²<br>Split Factor : 7<br>Individual Threshold : 0.4<br>Contrast : > 0.1 | Output Population : S/G2/M |
| **Find Cells (2)** | **Channel :** BP600/37 (2)<br>**ROI :** Whole Image<br>**ROI Region :** Whole Image Region | **Method :** B<br>Common Threshold : 0.05<br>Area : > 60 µm²<br>Split Factor : 7<br>Individual Threshold : 0.4<br>Contrast : > 0.1 | Output Population : G1 |
| **Find Cells (3)** | **Channel :** BP600/37 (2)<br>**ROI :** S/G2/M<br>**ROI Region :** Cell | **Method :** B<br>Common Threshold : 0.4<br>Area : > 100 µm²<br>Split Factor : 7<br>Individual Threshold : 0.4<br>Contrast : > 0.1 | Output Population : G1 + S/G2/M |
| **Select Cell Region** | **Population :** S/G2/M | **Method :** Resize Region [%]<br>Region Type : Nucleus Region<br>Outer Border : -60 %<br>Inner Border : 0 % | Output Region : Cytosol S/G2/M |
| **Select Cell Region (2)** | **Population :** G1 | **Method :** Resize Region [%]<br>Region Type : Nucleus Region<br>Outer Border : -60 %<br>Inner Border : 0 % | Output Region : Cytosol G1 |
| **Select Cell Region (3)** | **Population :** G1 + S/G2/M | **Method :** Resize Region [%]<br>Region Type : Nucleus Region<br>Outer Border : -60 %<br>Inner Border : 0 % | Output Region : Cytosol double pos |
| **Calculate Intensity Properties** | **Channel :** BP676/29 (4)<br>**Population :** S/G2/M<br>**Region :** Cell | **Method :** Standard Median | Output Properties : Intensity Nuclei S/G2/M |
| **Calculate Intensity Properties (2)** | **Channel :** BP676/29 (4)<br>**Population :** G1<br>**Region :** Cell | **Method :** Standard Median | Output Properties : Intensity Nuclei G1 |

| | | | |
|---|---|---|---|
| **Calculate Intensity Properties (3)** | **Channel :** BP676/29 (4)<br>**Population :** S/G2/M<br>**Region :** Cytosol S/G2/M | **Method :** Standard Median | Output Properties : Intensity Cytosol S/G2/M |
| **Calculate Intensity Properties (4)** | **Channel :** BP676/29 (4)<br>**Population :** G1<br>**Region :** Cytosol G1 | **Method :** Standard Median | Output Properties : Intensity Cytosol G1 |
| **Calculate Intensity Properties (5)** | **Channel :** BP676/29 (4)<br>**Population :** G1 + S/G2/M<br>**Region :** Cell | **Method :** Standard Median | Output Properties : Nuclear uptake Cas9 double pos cells |
| **Calculate Intensity Properties (6)** | **Channel :** BP676/29 (4)<br>**Population :** G1 + S/G2/M<br>**Region :** Cytosol double pos | **Method :** Standard Median | Output Properties : Intensity Cytosol double pos BP676/29 (4) |

**Define Results**

**Method :** List of Outputs
**Population : Whole Image**
Number of Objects
Apply to All :

**Population : S/G2/M**
Number of Objects
Apply to All :
Intensity Nuclei S/G2/M
Median : Mean+StdDev
Intensity Cytosol S/G2/M
Median : Mean+StdDev

**Population : G1**
Number of Objects
Apply to All :
Intensity Nuclei G1 Median : Mean+StdDev
Intensity Cytosol G1 Median : Mean+StdDev

**Population : G1 + S/G2/M**
Number of Objects
Apply to All :
Nuclear uptake Cas9 double pos cells Median : Mean+StdDev
Intensity Cytosol double pos BP676/29 (4) Median : Mean+StdDev

**Method :** Formula Output
Formula : a/a+b
Population Type : Objects
Variable A : S/G2/M - Number of Objects
Variable B : G1 - Number of Objects
Output Name : Percentage cells in S/G2/M

**Method :** Formula Output

Formula : a/b
Population Type : Objects
Variable A : G1 + S/G2/M - Nuclear uptake Cas9 double pos cells Median Mean
Variable B : G1 + S/G2/M - Intensity Cytosol double pos BP676/29 (4) Median Mean
Output Name : N/C Double Positive Cells

**Population : Whole Image :** None
Population : S/G2/M : None
Population : G1 : None
Population : G1 + S/G2/M : None

Acapella version: 4.1.1.117254. Timestamp: 2022-10-21 15:20:34 +0200.